

ver.Sep.20; accepted to AJ

Subaru Deep Survey III. Evolution of Rest-Frame Luminosity Functions Based on the Photometric Redshifts for K' -band Selected Galaxy Sample¹

Nobunari Kashikawa^{2,3}, Tadafumi Takata⁴, Youichi Ohyama⁴, Michitoshi Yoshida^{2,5}, Toshinori Maihara⁶, Fumihide Iwamuro⁶, Kentaro Motohara⁷, Tomonori Totani^{8,9}, Masahiro Nagashima⁹, Kazuhiro Shimasaku^{10,11}, Hisanori Furusawa⁴, Masami Ouchi¹⁰, Masafumi Yagi², Sadanori Okamura^{10,11}, Masanori Iye^{2,3}, Toshiyuki Sasaki⁴, George Kosugi⁴, Kentaro Aoki⁴, Fumiaki Nakata¹⁰

kashik@naoj.org

ABSTRACT

We have constructed very deep K' -selected multi-color $BVRIZ'JK'$ sample of 439 field galaxies. Based on this multi-color data, a photometric redshift for each sample galaxy was estimated. The overall redshift distribution $N(z)$ for

¹Based on data collected at Subaru Telescope, which is operated by the National Astronomical Observatory of Japan.

²Optical and Infrared Astronomy Division, National Astronomical Observatory, Mitaka, Tokyo 181-8588, Japan

³Department of Astronomy, School of Science, Graduate University for Advanced Studies, Mitaka, Tokyo, 181-8588, Japan

⁴Subaru Telescope, National Astronomical Observatory, 650 N. Aohoku Place, Hilo, HI 96720, USA

⁵Okayama Astrophysical Observatory, National Astronomical Observatory, Kamogata, Okayama 719-0232, Japan

⁶Department of Astronomy, Kyoto University, Kitashirakawa, Kyoto 606-8502, Japan

⁷Institute of Astronomy, University of Tokyo, Mitaka, Tokyo 181-8588, Japan

⁸Princeton University Observatory, Peyton Hall, Princeton, NJ08544, USA

⁹Theoretical Astrophysics Division, National Astronomical Observatory, Mitaka, Tokyo 181-8588, Japan

¹⁰Department of Astronomy, University of Tokyo, Hongo, Tokyo 113-0033, Japan

¹¹Research Center for the Early Universe, University of Tokyo, Hongo, Tokyo 113-0033, Japan

$K' \leq 21.0$ sample is consistent with previous observations, and we for the first time derive the $N(z)$ down to $K' = 24.0$. Taking account of the dust extinction and selection effects of the sample, the observed $N(z)$ distribution is well described with the PLE model, while the hierarchical galaxy formation model shows an apparent deficiency of galaxies especially at $z \gtrsim 2$. The photometric redshift and the best-fit SED model evaluations allow the derivation of the rest-frame K' , B , and $UV(2000\text{\AA})$ band luminosity functions and their evolutions. The rest K' -band luminosity function shows almost no evolution up to $z = 3$, while the rest- B luminosity function show mild luminosity evolution, and the rest- UV luminosity function show strong luminosity evolution. These findings seem to be qualitatively in favor of the PLE model. No evolution on rest K' -band luminosity function can also be consistent with the hierarchical galaxy formation model if M/L_K decreases with redshift, that is, the number density of K' -band luminosity selected galaxies does not significantly change with redshift while the number density of stellar-mass selected galaxies decreases with look-back time. This trend corresponds to the evolution of the rest $UV(2000\text{\AA}) - K'$ color, which gets bluer with increasing redshift. We also found that more massive galaxies are redder in this rest-frame color in every epoch. The rest- UV luminosity function of our K' -selected galaxies shows much shallower faint end slope at $z = 3$ than that of previous estimations for rest- UV selected Lyman break galaxies. As a consequence, the contribution to the global star formation rate of our K' -selected galaxies is about 42% of that derived from the integration of luminosity function of Lyman break galaxies at $z = 3$. The result suggests a possibility that large fraction of the star formation rate density at $z > 1.5$ comes from the contribution from the faint ($M_{2000} > -20$) blue galaxy population at high- z universe which have not yet obviously been identified.

Subject headings: cosmology: observations — galaxies: evolution — galaxies: luminosity function, mass function

1. Introduction

The large galaxy sample with redshift determined to faint magnitudes allows us to understand the evolution of galaxies. Previous deep spectroscopic surveys have shown several evolutionary trends for galaxies at $0 \lesssim z \lesssim 1$, especially on the evolution of luminosity functions (LFs), which is one of the fundamental observational tools to trace the galaxy evolution. Lilly et al. (1995) have shown that the LF for red galaxies does not evolve

significantly over $0 \lesssim z \lesssim 1$, which infers that red massive galaxies must have already been assembled by $z = 1$. On the other hand, their blue subsample is evolving, which indicates that they are formed later than the red subsample. Cowie et al. (1996) have shown the evidence of the “downsizing” trend in which more massive galaxies appear to be forming at higher redshifts.

Although it is important to see these evolutionary trends to the earlier epoch beyond $z = 1$, it is difficult to construct a large galaxy sample in familiar optical wavelength except for the distinct high- z star-forming populations of Lyman break galaxies and/or Ly α emitters at $z \gtrsim 3$ (Steidel et al. 1999; Ouchi et al. 2002, Paper II). There are some possible interpretations of such luminous high- z galaxies such as a core of today’s massive $L > L^*$ galaxies (Steidel et al. 1996) or as a low-mass starbursting building blocks of more massive galaxies seen today (Lowenthal et al. 1997). However, it remains uncertain how these $z > 3$ galaxies are related to present-day galaxies.

One of the explicit difficulties in tracing systematically the evolution of galaxies is that a single observed-frame does not correspond to a single rest-frame over wide redshift range, say $0 \lesssim z \lesssim 3$. The rest-optical frame in which we have seen the evolution trend at $0 \lesssim z \lesssim 1$ shifts to NIR region at $z \gtrsim 1.5$. An observation in wide wavelength range is undoubtedly required to know the SEDs of galaxies in order to follow their evolution based on the same rest-frame in which we can draw almost similar stellar contents at any redshifts.

There are two approaches to probe the rest-frame luminosity of galaxies. One is to change the observed band according to follow the redshifting rest-frame. This straightforward approach was taken by many studies. Cowie, Songaila, & Barger (1999) traced the rest- B band up to $z = 1$ by $UBVI$ multi-band observation. Furusawa et al. (2002, Paper IV) used a multi-color $BVRi'z'$ bands and traced the rest- B band LF up to $z = 1.25$. NIR photometry for Lyman break galaxies enables to derive their rest- V band luminosity at $z = 3$ (Shapley et al. 2001). This approach gives a reliable way to trace the rest-frame directly, though the study is restricted to a single rest-band. The other approach is to utilize the best-fit SED templates determined on photometric redshift method (Sawicki, Lin & Yee 1997; Rudnick et al. 2001). As have been already mentioned by many authors, the photometric redshift technique has less precision for redshift estimate than spectroscopic redshift. However, spectroscopic redshifts are practical only for bright objects. Photometric redshifts can be extensively applied to fainter objects with a fair degree of confidence. It is also of great use in constructing a statistically large sample in the redshift range between $z = 1.5$ and $z = 2.5$ where redshifts can be identified only by NIR spectroscopy. It works predominantly as a statistical technique rather than as constraints on parameters that determine the SED of an individual object. Studies based on the photometric redshifts and

that on the spectroscopic redshifts are complementary each other. If the SED of each sample galaxy in wide wavelength is given, the rest-frame luminosity of the galaxy can be estimated. This method has an advantage to derive the rest-frame luminosity at any redshift and at any wavelength, though the estimated luminosity inherits an uncertainty in determining the photometric redshift.

In this study, we have constructed a very deep K' -band selected sample of galaxies. We then adopt the second approach described above with photometric redshifts derived from multi-color $BVRIz'JK'$ deep images and investigate the evolution of the LFs in the three (K' , B , and UV) rest-frame bands out to $z = 3.5$ where the K' -band still traces the rest wavelength longer than an age-sensitive spectral break at 4000Å.

NIR band selected samples may provide significant advantages over optical-band selected samples in studying galaxy evolution due to smaller extinction by dust and less type-dependent k -corrections (Mannucci et al. 2001) at these wavelengths. Moreover, NIR selection provides samples which are not biased towards star-forming galaxies and allows to estimate the mass of galaxies over a wide range of redshift (Saracco et al. 2001). NIR photometry in general improves the estimate of photometric redshift (e.g., Bolzonella, Miralles, & Pello 2000).

The Subaru Deep Field (SDF) was imaged quite deeply at near-infrared with wide field near infrared camera CISCO and yielded some of the faintest galaxies ever observed, down to magnitudes of $J = 25.5$ and $K' = 24.5$ (Maihara et al. 2001, Paper I), which is much deeper than most of previous K' -band surveys (e.g., Cowie et al. 1996; Barger et al. 1999; Fontana et al. 2000; Rudnick et al. 2001). The field was well selected with care to avoid large Galactic extinction and nearby clusters of galaxies and to get smaller airmass than HDF at Mauna Kea (Paper I). The following optical imaging enabled us to estimate the photometric redshifts of these faint objects and offered the discovery of faint high- z object candidates. In the SDF, we have already evaluated the number counts in J - and K' -bands, near-infrared color distribution, and contribution to Extragalactic Background Light (Paper I, see also Totani et al. 2001a). Totani et al. (2001b) have investigated a detailed comparison of the number counts, colors, and size distribution for the SDF galaxies with theoretical galaxy formation models. Nagashima et al. (2002) have also analyzed the SDF galaxies by using a semi-analytic model of galaxy formation based on the CDM model. In this paper, we will compare the redshift distribution with their models.

This paper will be organized as follows. We present the process to construct the K' -limited sample of SDF galaxies and the estimation of photometric redshifts as well as their spectroscopic calibration in §2. In §3, we show the redshift distribution of our sample and compare it with galaxy formation models. We discuss the evolution of LFs on rest K' , B ,

and UV(2000Å) bands in §4 and the evolution of rest $UV-K'$ color in §5. We will also describe in §6 the evaluation of star formation rate density (SFRD) derived from our LF estimate. We give a summary them in §7. Throughout this paper we assume a flat, matter dominated universe ($\Omega_m = 1$) with $H_0 = 75\text{km}\text{s}^{-1}\text{Mpc}^{-1}$ to compare with other major previous observations.

2. K' -band selected Galaxy Sample

2.1. The Data

We have used a deep multi-color data set of $BVRIZ'JK'$ images taken with Subaru telescope on the Subaru Deep Field. The SDF is centered on $\alpha = 13^h24^m21.^s38$; $\delta = +27^\circ29'23.^''0$ (J2000). The J and K' imagings, data reductions are described in the previous paper (Paper I). The optical follow-up imaging observations were carried out during the commissioning runs of the FOCAS (Kashikawa et al. 2000) and Suprime-Cam (Miyazaki et al. 1998) on February to June, 2001. In this study, we used the Johnson B , Kron-Cousins R and I bands images taken with FOCAS and Johnson V and SDSS z' band images taken with Suprime-Cam. The observation and data reduction of the V and z' data, which are one of the wide field imaging data for the SDF, will be described in coming paper (Shimasaku et al. 2002; Furusawa et al. 2002, Paper IV). Here we briefly describe the imaging data of B , R , and I taken with FOCAS.

FOCAS has a field of view as large as $6'\phi$ which could entirely cover not only the SDF $2' \times 2'$ itself but also its flanking fields. The SDF has flanking fields which is $5'$ square size in total surrounding the SDF, though their limiting magnitude in K' ($K' \leq 20.5$) is fairly shallower than that of the central field. FOCAS has a couple of 2048×4096 pixel CCD chips with the pixel scale of 0.103 arcsec/pix . The typical seeing size was $0.6 - 0.8\text{ arcsec}$. The total integration time was 2.5hr, 4hr, and 1hr for B , R , and I bands respectively.

The B , R , and I images were reduced in a standard manner. After flat-fielding, we have corrected the image distortion caused by the optics of FOCAS and the telescope. The undistorted images have accuracy of 1.0 pix r.m.s. This distortion pattern has been confirmed to be independent of the flexure of the telescope and the instrument. The image shift caused by the flexure was about 0.6 pix within the maximum exposure time of 30min. Relative sensitivity of two CCDs was corrected based on the difference of sky brightness assuming that the sky is uniform over the field of view. Actually, the relative ratios of sky brightness of two CCDs on the same exposure were stable with 1% fluctuation. The sky was determined by fitting the unvignetted area of each frame with two dimensional 3rd or 4th

order polynomials and subtracted. The relative shifts and rotations among dithered frames were measured and fixed using the positions of several point sources. Then they were stacked each other using the IMCOMBINE task in IRAF. Magnitude zero points were calibrated to the Johnson-Cousins system using Landolt photometric standard stars. The accuracy of the zero-points are estimated to be in the range $0.03 - 0.08$ mag. The magnitudes have also been corrected for the Galactic absorption, using $E(B - V) = 0.018$ derived from Schlegel, Flinkbeiner & Davis (1998), yielding $A_B = 0.074$ mag, $A_V = 0.056$ mag, $A_R = 0.046$ mag, $A_I = 0.033$ mag, $A_{z'} = 0.025$ mag, $A_J = 0.015$ mag, and $A_{K'} = 0.006$ mag.

The summary of optical imaging data used in this study is presented in Table 1. The 5σ limiting magnitudes in Vega system within $2.^{\circ}0$ aperture for these images are $B \leq 28.08$, $V \leq 26.28$, $R \leq 27.88$, $I \leq 25.93$, $z' \leq 24.27$, $J \leq 25.11$, and $K' \leq 23.73$.

Among seven images, the J -band image has the smallest area of $2' \times 2'$ on which the deepest K' -band data exists. Therefore we first rescaled all the data to the same pixel scale ($0.^{\circ}103$ /pix) of the B , R , and I data, corrected relative rotation based on the positions of several bright point sources, and extracted the $1.^{\circ}90 \times 1.^{\circ}97$ region common to the J and K' -band images for further analysis. The error of this image translation was below 0.02 arcsec.

2.2. Object Detection and Photometry

We have extracted objects using SExtractor (Bertin & Arnouts 1996). The objects are extracted from the K' -band image as a reference image and photometric measurements are performed on the other image for the exact positions where sources were detected on the reference image. We choose a 4.0pix FWHM Gaussian convolution kernel in object detection on the reference K' -band image. We used a detection threshold of 24.1 mag/arcsec 2 corresponding to the 1.5σ above the background noise level in K' -band which is the same as in Paper I.

To measure colors of detected objects, aperture photometry was carried out for seeing-corrected images, which was created by convolving Gaussian filters in order to match the seeing size to that of the V -band which is the largest among the seven images. At first we used a fixed aperture. However, it was difficult to choose an adequate aperture size because photometry with large aperture is affected by close neighboring objects while small aperture does not cover the same physical sizes for both nearby objects and distant objects at the same time. Finally we have chosen an aperture size adjusted for each object size but kept identical for all the seven images. In order to choose the adequate aperture size

in deriving colors of objects, we have tried many times for different aperture sizes and confirmed the consistency between the resulting photometric redshifts and spectroscopic redshifts for calibration samples (see Section 2.3). We found a $2 \times \text{FWHM}$ (FWHM was measured on K' -band image) aperture for each object is the optimum aperture size to derive correct photometric redshifts. In this way, we have measured total magnitudes (“`MAG_BEST`” magnitudes from SExtractor), $2 \times \text{FWHM}$ aperture magnitudes for all the seven images. It should be noted that the $2 \times \text{FWHM}$ aperture magnitude is only used for SED fitting in deriving the photometric redshift, and further analysis are based on the total magnitude. The 9 objects which have $\text{stellarity} > 0.9$ with $K' \leq 23.0$ were eliminated as Galactic stars from our galaxy sample. We have also removed 12 objects whose photometry is strongly affected by nearby bright stars in any of the seven band images.

Our final K' -selected catalog contains 439 objects with the magnitude limit of $K'_{\text{tot}} \leq 24.0$. According to Paper I, the completeness is over 70% at this limiting magnitude.

2.3. Photometric Redshifts

We used the publicly available *Hyperz* code by Bolzonella, Miralles, & Pello (2000) to determine photometric redshifts for our seven band $BVRIz'JK'$ photometry. The *Hyperz* code derives a photometric redshift for each input multi-photometry set according to the standard SED fitting minimization procedure. The detail of the method as well as discussions about the accuracy of evaluated redshifts are presented in Bolzonella, Miralles, & Pello (2000), therefore we describe here briefly about our choices of major input parameters. We used five (Burst, E, Sa, Sc, and Im) synthetic galaxy SED templates of Bruzal & Charlot model (GISSEL98, Bruzal & Charlot 1993) to compare with the observed SED. The default SED templates applied in *Hyperz* assume the Miller & Scalo IMF from $0.1M_{\odot}$ to $125M_{\odot}$, the solar metallicity $Z = Z_{\odot} = 0.02$, ages ranging from 10^6 yr to 2×10^{10} yr, and Madau (1995)’s formula for continuum depression due to the intergalactic absorption blueward of Lyman α emission. The adopted SED templates are assumed for an instantaneous single-burst SFR model for “Burst” SED, and exponentially decaying SFRs with e -folding timescales of 1, 3, 15 Gyr and infinity (*i.e.*, constant SFR) to match the colors of present-day galaxies of different spectral types from “E” to “Im”. Though three more additional spectral type templates can be applied in *Hyperz*, the accuracy for photometric redshift z_{phot} estimate was found to be unchanged when applying all the 8 templates. We have chosen a Calzetti et al. (2000)’s extinction law with A_V ranging between 0.0 and 1.8. The step in redshift in searching the solutions between $z = 0$ and $z = 7$ is $\Delta z = 0.1$, though the resolution in the final minimization is 10 times better. The results are not significantly affected by the choice

of smaller Δz . We have also applied the constraint on the age of the template to be less than the age of the universe at the redshift under consideration. The transmission curve for a given filter set was defined based on the real measured curve for each instruments. An uncertainty of derived photometric redshift for each object was estimated from χ^2 probability distribution with the confidence level at 90% derived in SED template matching, which will be shown later. As expected, the error becomes larger as K' magnitude goes fainter.

We examined the accuracy of our determination of photometric redshifts, z_{phot} , against spectroscopic redshifts, z_{spec} . We have measured spectroscopic redshifts for 76 galaxies in $5' \times 5'$ field centered on SDF. All these spectroscopic data were taken during the commissioning runs of FOCAS MOS mode in April and May, 2001. The spectra cover $4700 - 9000\text{\AA}$ with a pixel resolution of 2.8\AA under the $0.^{\circ}8 - 1.^{\circ}0$ seeing size and were reduced in a standard manner.

In this $5' \times 5'$ SDF flanking fields, J -band data is not available except for the central $2' \times 2'$ region and K' -band image has shallower limiting magnitudes of $K' < 20.5$. Five galaxies out of 76 galaxies belong to the SDF central field in which J -band photometry is available. We have confirmed an excellent agreement of the estimated of z_{phot} between the photometric data sets with and without J -band for these 5 galaxies. The comparison of z_{phot} to z_{spec} for our spectroscopic sample is shown in Figure 1, in which we found good agreement, though we don't have enough spectroscopic galaxy sample at $1.5 < z$. The mean error is $\Delta z = \langle z_{spec} - z_{phot} \rangle = -0.038$ with $\sigma = 0.207$. The large inaccuracy seen in $z \leq 0.4$ would be caused by the lack of U -band photometry which can detect a Balmer break at this redshift range. If objects with $z < 0.4$ are removed, the accuracy improves to $\sigma = 0.178$. Note that we don't have any apparent catastrophic errors, though the spectroscopic sample itself is small. If five objects with $\Delta z > 0.4$ are removed, the accuracy improves to $\sigma = 0.160$.

3. Redshift Distribution

We describe in this section the derived redshift distributions of our sample. Figure 2 shows the K' - z relation. The error bars of determined z_{phot} are estimated from χ^2 probability distribution with the confidence level at 90% derived in SED template matching. Figure 3 shows the redshift distribution of our K' -selected sample. The distribution has a peak around $z = 0.8$ which is slightly larger than the $N(z)$ peak around $z = 0.5 - 0.6$ derived by Fontana et al. (1999) or Rudnick et al. (2001) for $K \lesssim 21$ samples which include HDF-N,S fields. However, if we restrict our sample to brighter galaxies having $K' \leq 21.0$, the peak moves slightly toward a lower z at $z = 0.6$. The number density of galaxies at $1 < z < 1.5$ is 4.8 galaxies/arcmin 2 at $K' \leq 21.0$, which is consistent with the result of Fontana et al. (1999)

of 4.4 galaxies/arcmin² at $K' \leq 21.0$. Thus, our $N(z)$ is consistent with those of Fontana et al. (1999) and Rudnick et al. (2001).

We can use this overall redshift distribution of K' -band selected galaxies to compare the predictions of theoretical models of galaxy formation. The redshift distribution for K -selected galaxy sample was first pointed out to be an effective tool to discriminate galaxy formation models by Kauffmann & Charlot (1998, KC98). The hierarchical clustering model, in which massive galaxies were assembled much more recently through merging of small galaxies, predicts less galaxy abundance at high- z ($z > 1$) than that expected from the pure luminosity evolution (PLE) model. The recent results of Fontana et al. (1999) and Rudnick et al. (2001) for $K' \leq 21$ sample were both consistent with the hierarchical clustering model. Since our K' -selected sample is much deeper than Fontana et al. (1999) and Rudnick et al. (2001) by 3mag, the derived redshift distribution reflects both high- z ($z > 2$) population and intrinsically faint population in local universe and is crucial and useful in reconciling observation with theoretical models. Actually, the fraction of galaxies at $z \geq 1.6$ detected in $K' \leq 21$ sample of Fontana et al. (1999) was only 9%.

Following the same manner as KC98 and previous observations, Figure 4 demonstrates the normalized cumulative redshift histogram for our K' -selected sample as well as the theoretical predictions of both PLE and hierarchical clustering models. The thick solid histograms show the results of observation, while other lines show the model predictions. We have carried out Monte Carlo realizations to see the distortion that the error of our derived photometric redshift could affect on the resulted $N(z)$. At first, we have created a “pseudo-galaxy-catalog” in which redshift of each galaxy was assigned to be the photometric redshift solution plus a random error perturbed in the range of confidence interval at 90% in the SED χ^2 fitting procedure (same as the error bars denoted in Figure 2). In this process, magnitude of each galaxy was also assigned with a random error perturbed within the measured photometric error by SExtractor. We assumed here that the error in photometric redshifts is independent of the photometric error, though a large photometric error would cause a large error of photometric redshift in most cases. The redshift distribution is re-calculated for this sample. We repeated 200 times of generating such pseudo-galaxy-catalogs and investigated the scatter of derived redshift distribution. The shaded regions in Figure 4 show the $\pm 3\sigma$ deviated counts estimated by this method.

The thick dotted lines show the PLE model by Totani et al. (2001b). The model normalizes its number density of galaxies at $z = 0$ by the B band luminosity function, and it probes the evolution backward in time. Galaxies are classified into six morphological types of E/S0, Sab, Sbc, Scd, Sdm, and the distinct population of dwarf elliptical galaxies. Their luminosity and SED evolutions are described by a standard galaxy evolution model of

Arimoto & Yoshii (1987) and Arimoto, Yoshii & Takahara (1992). All galaxies are simply assumed to be formed at a single redshift $z_F = 5$. A reasonable evaluation of dust extinction by a screen model, and selection effects such as cosmological dimming of surface brightness are taken into account. The detail of the model is described in Yoshii (1993) and Totani & Yoshii (2000). Their selection criteria for object detection are completely the same as ours and Paper I. This PLE model, which takes account of the two distinct populations of giant elliptical galaxies and dwarf elliptical galaxies, was found to match extremely well with the observed K -band galaxy counts on the SDF beyond $K > 22.5$ where the PLE model with a single elliptical population could not explain the observed galaxy abundance. In their original model of Totani et al. (2001b) they have predicted the $N(z)$ for the SDF based on an isophotal magnitude in which selection effects are easy to be taken into account. We recalculated the $N(z)$ predicted by the model based on a total magnitude in this study.

On the other hand, the thick dashed lines represent the semi-analytic hierarchical galaxy formation model by Nagashima et al. (2002). The model is based on the structure formation theory in the CDM model, which corresponds to the hierarchical clustering of dark halos, and contains some important physical processes concerned with the evolution of the baryonic components such as gas cooling, star formation, supernova feedback and galaxy mergers. In this model, merging histories of dark halos are realized by using a Monte Carlo method assuming a power spectrum of initial density fluctuation in a Gaussian random field, and then, the above baryonic processes are followed in each dark halo. Thus star formation histories, luminosities and colors of individual galaxies are predicted with this model. The details of the model itself is presented in Nagashima et al. (2001) in which the model well reproduces the local luminosity function, the H I gas mass fraction, galaxy sizes and so on. The Nagashima et al. (2002) model employed in this study improves the Nagashima et al. (2001) model by taking account of almost the same selection effects as Totani et al. (2001b) and dust extinction, and can predict the consistent number counts of galaxies with that of observed on the SDF. Note that the model of Totani et al. (2001b) was calculated in a cosmology with $\Omega_m = 0.2$ and $\Omega_\lambda = 0.8$ and that of Nagashima et al. (2002) with $\Omega_m = 0.3$ and $\Omega_\lambda = 0.7$ as are those of their original models, whereas an overall distribution of observed photometric redshift does not depend on cosmology. In the brightest $19 < K' \leq 21$ bin, we also overlay the model predictions of KC98's PLE and hierarchical clustering model for comparison.

It should be noted that the hierarchical clustering model apparently shows a strong deficiency compared with the observed $N(z)$ especially at high redshifts ($z > 2$). In $22 < K' \leq 23$ bin which contains 119 sample galaxies and still attains the completeness of 100%, the PLE model agrees with the observed count better than hierarchical galaxy formation model. The PLE model can account for the abundance of the high- z ($z > 2$) galaxies. On

the other hand, its underprediction of the high- z galaxy abundance as compared to KC98's PLE model is attributed to the dust evaluation in the model.

We performed two-sample form of the Kolmogorov-Smirnov test (K-S test) to see the statistical agreement between observation and models. The chance probability as well as the χ^2 values (in parentheses) are listed in Table 2. The K-S test accepts the hypothesis that the observation and the PLE model in $19 < K' \leq 23$ bins are drawn from the same distribution with 1% significant level, while the hierarchical galaxy formation model agrees with observation only in the bright $19 < K' \leq 22$ bins. In the faintest $23 < K' \leq 24$ bin both of the model predictions are found to be different from the observation. In this bin, the observed count shows a high- z tail which may be produced by both effects that there are more galaxies at high- z and less galaxies at low- z than models. Though the error shaded regions seem to distribute below the observed counts, it is partly because the pseudo-galaxy-catalog lacks the objects whose reassigned magnitudes are beyond the limiting magnitude $K' = 24.0$. Note that the completeness of the sample is 100% at $K' = 23.5$, though 70% at $K' = 24.0$ (Paper I). In the galaxy count, the model prediction begins to show a slight deviation from the observation at this faint magnitude (Totani et al. 2001b; Nagashima et al. 2002). The discrepancy in this faintest bin is presumably caused by the large photometric errors which give incorrect solutions of photometric redshifts. More detailed refinements of the model may also be required.

As noted above, previous works on KC98 test such as Fontana et al. (1999) and Rudnick et al. (2001) has resulted that their $N(z)$ is well described with the hierarchical clustering model prediction and that the PLE model overpredicts the abundance at all redshifts. Our observed $N(z)$ itself is consistent with those observed by Fontana et al. (1999) and Rudnick et al. (2001) at least at $K' \leq 21$, and KC98 test with our $N(z)$ would give the same conclusion if we adopt the model predictions of KC98. In this study, we introduce more realistic models of PLE and hierarchical galaxy formation model which takes account of both the selection effects of the sample and dust extinction, and found that the PLE model is favored by the observed $N(z)$, while the hierarchical galaxy formation model prediction is substantially below the observed $N(z)$ at high- z . It might suggest that we need some additional physical processes in the CDM model. We note, however, that the result is obtained on the very small field of the sky, thereby it should be confirmed with future wide-area K -selected sample.

4. Evolution of Rest frame Luminosity Functions

Using the estimated photometric redshift catalog, we now investigate the galaxy population and its evolution by means of luminosity functions. Our wide wavelength coverage

and SED estimation for each sample galaxy allow us to derive LFs in the three rest-frame of K' -, B -, and UV(2000Å)-bands. We will investigate the evolution of rest-frame LFs at $z < 3.5$ where K' -band traces the rest-frame wavelength longer than 4000Å. Though it is quite interesting to see the difference of rest-frame LFs for blue/red subsample (e.g., Lilly et al. 1995) or spectral type (e.g., Folkes et al. 1999) subsample, our sample is not so large as to be subdivided into small subsamples with enough statistical confidence. Such a detailed analysis would be possible in the future when large NIR imaging survey is carried out.

4.1. Rest K' frame Luminosity Function

First, we derive the rest- K' band luminosity functions. For each galaxy we have determined a rest-frame absolute K' magnitude, $M_{K'}$ as

$$M_{K'} = m_{K'} - 5\log(d_L/10\text{pc}) - k(z), \quad (1)$$

where d_L is the luminosity distance and $m_{K'}$ the apparent K' magnitude. The k -correction $k(z)$ can be derived from the best fit SED template for each galaxy.

To determine the LFs we use a traditional $1/V_{max}$ method (Felten 1977).

$$\phi(M)dM = \frac{4\pi}{d\omega} \sum \left[\int_{z_{min}}^{z_{max}} \frac{dV}{dz} dz \right]^{-1}, \quad (2)$$

where dV/dz is the comoving differential volume. The limits z_{min} and z_{max} are defined as the smallest and the largest redshifts that a given galaxy could be at and still make it included into a sample (see detail in Ellis et al. 1996). The sum is carried out over all galaxies in the sample lying within the specified range of redshift and magnitude. The volume is based on an effective solid angle, $d\omega$, of the survey of 3.739 arcmin².

The rest- K' frame LFs for four redshift intervals at $0.6 < z \leq 3.5$ are shown in Figure 5. We have neither enough sample galaxies to derive a reliable LF nor good accuracy in redshift identification at $z < 0.6$, so we omit this redshift interval. Instead, we refer the local K -band LF derived by Loveday (2000) for Stromlo-APM Redshift Survey shown as a dotted line on each frame in Figure 5. Although Loveday (2000)'s sample is smaller than another local K -band LF of 2dF survey (Cole et al. 2001), it extends to so faint magnitude as $M_K = -16$ with smaller statistical error which is adequate to compare with our sample. The error bars show the statistical uncertainties evaluated from a bootstrap resampling method with a

series of 500 Monte Carlo simulations. We fit the LF by a usual Schechter parameterization and list the best fit parameters in Table 3.

The derived K' -LF at $0.6 < z \leq 1.0$ slightly differ from local one having hints of steeper faint end slope and brighter bright end, though the overall shape of the LF seem to agree with that of local K' -band LF taking account of the normalization difference. The most striking result perceived from this figure is that K' -band LF remains almost unchanged from $z = 0.6(0.0)$ to $z = 2.5$ and shows decline at the bright end at $2.5 < z \leq 3.5$. We have evaluated the robustness of our resulted LFs against the errors of our photometry and photometric redshift estimate by the Monte Carlo realizations which is as same as that we performed in §3. The evaluated 1σ scatter of derived LF parameters, *i.e.*, α , M^* , ϕ^* are denoted in Table 3. We found that the effects of photometric and redshift errors are small with negligible effect on α , and 0.5mag at most in M^* . The K' -band LF at $2.5 < z \leq 3.5$ has also a sign of steeper faint end slope than that at lower-z ones, which is expected in the context of the hierarchical clustering model. However, the trend may not be statistically significant due to the lack of enough sample in faint ($M_{K'} > -21$) bins.

Cowie et al. (1996) have derived the rest K' -band LF for $0.6 < z < 1.0$ galaxies. It remains almost unchanged from that for $0 < z < 0.2$. Drory et al. (2001) also showed no significant evolution of rest K' -band LF for $z < 1.2$. Lilly et al. (1995) have also noted that rest-frame red luminosity galaxies have a weak evolution up to $z = 1$. This trend has found to continue up to $z \lesssim 3$ in this study. The almost no evolution in rest K' -band LF infers that the old stellar population in galaxies was already in place by $z = 2 - 3$ and their stellar mass did not change significantly at $0 < z < 3$. It seems that the present result is inconsistent with hierarchical clustering model. Papovich, Dickinson, & Ferguson (2002) estimated the stellar masses for the HDF-N galaxies with population-synthesis models and have found that massive, present-day galaxies were not fully assembled by $z \sim 2.5$ as predicted by hierarchical galaxy formation model, which might be also inconsistent with ours. However, Drory et al. (2001) have shown that the M/L_K slightly decreases with redshift at $z < 1.2$. If this trend continues up to $z \sim 2.5$, all the findings are consistent that the number density of K' -band luminosity selected galaxies does not remarkably change with redshift while the number density of stellar-mass selected galaxies decreases with look-back time.

It should be noted that we are assuming here a rather large extrapolation along the SED template from the observed K' -band to the rest K' -band especially at $2.5 < z \leq 3.5$. The reliability of this extrapolation depends on some appropriate assumptions in constructing the SED templates based on our fundamental knowledge of star formation histories in a galaxy. Recently, Shapley et al. (2001) and Papovich, Dickinson, & Ferguson (2002) have attempted to derive the stellar masses for individual sample of Lyman break galaxies at

$z \sim 3$. In these studies, their UV to near-IR photometries were fitted with a series of stellar population synthesis models, which is basically the same SED fitting method as photometric redshift except that they considered carefully almost full allowable range of various input parameters in constructing SED templates. This constraint method can only be applied to the sample whose redshifts are reliably determined by spectroscopy. Although some interesting trends have been found among parameters of star formation histories, they found only loose constraints on each of the parameters including stellar masses. This means that stellar mass measurement even at observed- K' band at $z \sim 3$ has some uncertainty. The most significant factor of uncertainty in deriving stellar mass is a second stellar-population component (Papovich, Dickinson, & Ferguson 2002) of old stars which have formed in a previous burst occurred before ongoing active star formation. The stellar masses with this second component model are estimated to be 3 – 8 times of that of the single component models. While this old population, if any, actually influences on the estimate of stellar masses, its allowable flux contribution is supposed to be small because of its high mass-to-light ratio. For example in Figure 19 of Papovich, Dickinson, & Ferguson (2002) showing the effect of second old stellar population on the galaxy SED, the second component increases the inferred rest- K' band luminosity in a factor of less than ~ 1.4 which corresponds to ~ 0.37 mag brightening. As a consequence, our extrapolation of SED and derived rest- K' band magnitudes at high- z in this study could have uncertainty to the same extent.

In the following subsections, we will see the evolution of rest-frame LFs of bluer rest-bands that trace young stellar population and sensitive to star formation activity.

4.2. Rest B frame Luminosity Function

We have also estimated the rest- B band luminosity functions with almost the same way of K' -LF. Six objects out of 439 K' -selected sample were not detected in the B -band image. We have derived their inferred B -band magnitudes from their best-fit SED templates convolved with a B -band response curve. The consistency between photometric B -band magnitudes and this inferred B magnitudes from their best fit SEDs were checked with sample galaxies except these six B -dropout galaxies, and their agreement was found to be within 0.56 mag r.m.s. The inferred B magnitudes of six B -dropout galaxies were all beyond the 1σ limiting magnitude 29.76 of the B -band image.

The rest- B band LFs at $0.6 < z \leq 3.5$ are shown in Figure 6 and the best fit Schechter parameters are listed in Table 3. Superimposed dotted lines are the local B -band LF from the SDSS (Blanton et al. 2001) converted from g^* -band. In the $0.6 < z \leq 1.0$ bin panel, we also superimposed as a dashed line $0.75 < z < 1.0$ rest B -band LF derived in CFRS (Lilly

et al. 1995) for the $\Omega_m = 1$, $\Omega_\lambda = 0$, and $h = 0.75$ case. Although CFRS only samples the bright end of the LF, the agreement between CFRS and our result for $0.6 < z \leq 1.0$ is quite well, both showing the brightening by 0.5 mag from the local rest- B LF. Note that CFRS is the I -band magnitude limited sample and ours is K' -band limited, though both of these bands trace above 4000Å at $z < 1.0$.

In the $2.5 < z \leq 3.5$ panel of Figure 6, the dashed line represents the rest V -band LF of Lyman-break galaxies at $z \sim 3$ by Shapley et al. (2001). We have converted their rest- V band magnitude to our rest- B band magnitude using the rough estimate of average color of observed $(H - K) \sim 0.40$, which approximately corresponds to rest $(B - V)$, at $z \sim 3$ derived on HDF-N galaxies by Papovich, Dickinson, & Ferguson (2002). We have also re-estimated the M_V^* and ϕ^* values assuming a cosmology with $\Omega_m = 1.0$ and $h = 0.7$. Though band conversion has some uncertainty ($\sim \pm 0.5$), our rest- B LF at $z \sim 3$ is in good agreement with that of Shapley et al. (2001) which is a part of Steidel et al. (1999)'s rest-UV and spectroscopic selected sample. The agreement of LFs at $z \sim 3$ of our K' -selected and their optical-selected samples means that there are very few, if they are present, red candidates of old non-star-forming galaxies that would not detected in optical bands but in near-infrared bands, which is also suggested by Shapley et al. (2001) and Papovich, Dickinson, & Ferguson (2002). On the contrary, we can conclude that our K' -selected sample has not a large deficit of young blue star-forming galaxies at least in brighter magnitudes.

In contrast to the rest- K' LF, the rest- B LF shows brightning with epoch up to $z < 2.5$. The bright end of the LF appears to continue brightening by 0.4mag from $0.6 < z \leq 1.0$ to $1.0 < z \leq 1.5$, and by a further 0.4mag from $1.0 < z \leq 1.5$ to $1.5 < z \leq 2.5$ with keeping the faint end slope constant, though its brightening degree is within the M^* error caused by photometric and redshift errors. The bright end amplitude of the rest- B LF at $1.5 < z \leq 2.5$ clearly exceeds over the local B -band LF, while it declines at $2.5 < z \leq 3.5$ almost to the local amplitude.

This brightening evolution in rest- B LF has also seen in Sawicki, Lin & Yee (1997) for the HDF F814W_{AB} < 27 sample. They have found not only the brightening but also the steepening of the faint end slope with increasing redshift to $z = 3$. The difference of faint-end slope is presumably caused by the difference of the observed band used to construct the magnitude limited sample, which will be discussed later.

In the rest- B band, we have found a strong luminosity evolution at $z < 3$ which was not seen in the rest- K' band. In next subsection, we further investigate this trend in bluer UV band which directly relates to the star formation rate of a galaxy.

4.3. Rest UV 2000Å frame Luminosity Function

We derive the rest-UV LF at 2000Å in which Sullivan et al. (2000) have derived the local LF for an ultraviolet selected sample. We have evaluated photometric redshifts as well as best-fit SEDs for all the galaxies in our K' -selected sample. Therefore we can derive absolute magnitudes of any rest wavelength in the AB system, although the derived magnitudes would suffer directly the error of the photometric redshift evaluation. Here we derive the absolute magnitude, $M_{AB(2000)}$ as follows,

$$M_{AB(2000)} = m_{AB} + 2.5\log(1+z) - 5\log(d_L(z)/10\text{pc}), \quad (3)$$

where m_{AB} is the observed redshifted magnitude at $2000(1+z)\text{\AA}$ and $d_L(z)$ is the luminosity distance. It is to be noted that derived rest-UV luminosity is uncorrected the dust extinction which is estimated to be in the range of $A_{1700} = 0.0 - 4.0\text{mag}$ at $z \sim 3$ (Papovich, Dickinson, & Ferguson 2002).

The rest-2000Å LFs at $0.6 < z \leq 3.5$ are represented in Figure 7 and best fit Schechter parameters are again listed in Table 3. Superimposed dotted lines are the local rest-2000Å LF (Sullivan et al. 2000) for $h = 0.75$ converted to AB system by a 2.29 mag offset (Cowie, Songaila, & Barger 1999). As was seen in the rest- B band LF, the rest-2000Å LFs also show a luminosity evolution which is stronger than in the rest- B LF and continues up to $2.5 < z < 3.5$ bin. The M_{2000}^* value is getting luminous from $z = 0.6$ to $z = 3.5$ over 1 mag, which is more significant than M_{2000}^* errors.

Cowie, Songaila, & Barger (1999) have derived the rest-2000Å LF at $0.5 < z < 0.9$ and $1.0 < z < 1.5$. We refer their LFs in the case of $\alpha = -1.0$ and $h = 0.75$ as dashed line in corresponding redshift bins of Figure 7. They mentioned that their lower value of ultraviolet luminosity density than other studies would partly be caused by field variation. Taking account of this normalization fluctuation as well as their fairly large error of $\pm 0.4\text{mag}$ in determination of M^* , our results agree with their LFs.

In the $2.5 < z \leq 3.5$ panel of Figure 7, the dashed line represents the rest 1700Å LF of Lyman-break galaxies at $\langle z \rangle = 3.04$ by Steidel et al. (1999). We ignore the rest-band difference between 2000Å and 1700Å because the correction would be less than $\delta M \simeq 0.13$. Again as seen in rest- B LF, our estimate of the rest-UV LF at $z \sim 3$ is in good agreement with that of Steidel et al. (1999) which have only estimated the bright end ($M_{1700} < -20$).

As has been noticed in rest- B band LF, we can see less faint galaxies at higher redshift in this rest-UV LF. This is probably caused by the fact that our K' -limited sample is insensitive to blue dwarf galaxies. The deficit of faint end galaxies in the K -selected sample is also seen

in local universe. The LF of K -selected sample (e.g., Cole et al. 2001, Table 3) have shallower faint end slope $\alpha \sim -1.0$ than that of optical-selected sample (e.g., Blanton et al. 2001) of $\alpha \sim -1.20$.

5. The Evolution of Rest Ultraviolet- K' Color

In previous section concerned with rest-frame luminosity functions, we found rest K' -band LF has almost no evolution, while the B - and the UV-band LF show drastic luminosity evolution, that is, galaxies get brighter in bluer band with increasing redshift. As a natural consequence, galaxies are inferred to be getting bluer in rest-frame with redshift. To see this trend more definitely, we show the rest $M_{2000} - M_{K'}$ color evolution with redshift in Figure 8. The rest-frame 2000Å and K' luminosity of each galaxy selected in K' -band can be calculated with the same manner described above. Note that this color estimate is not based on the same aperture magnitudes in 2000Å and K' bands. We categorized the sample galaxies according to their absolute rest K' -band magnitudes $M_{K'}$, which are fairly good indicators of the stellar mass. We have mentioned in §4.1 that $M_{K'}$ derived from the extrapolation of SED template might be a poor proxy of stellar mass at $z \sim 3$ as suggested by Shapley et al. (2001) and Papovich, Dickinson, & Ferguson (2002). Though predominant uncertainty caused by the second old population would increase the absolute stellar mass estimate systematically, the correlation between $M_{K'}$ and stellar mass would be retained if all the galaxies at $z \sim 3$ are assumed to have similar mass ratios of the young-to-old stellar populations. It was found that the derived stellar masses have a fairly tight correlation with extinction-uncorrected rest- V luminosity (Shapley et al. 2001). Papovich, Dickinson, & Ferguson (2002) have also found the correlation even with the rest-UV luminosity with a scatter of ~ 0.3 dex, though Shapley et al. (2001) have found only weak correlation. However, we should note again that the extinction is still uncertain in the UV luminosity at $z \sim 3$. In Figure 8, The most massive $M_{K'} \leq -23.5$ sample is represented with open circles. $-23.5 < M_{K'} \leq -21.0$ and $-21.0 < M_{K'}$ samples are represented by small filled circles and cross-dots, respectively. The median $M_{2000} - M_{K'}$ color for each redshift is traced by solid, dotted and dashed lines from massive sample to less massive one respectively.

Two significant trends can be seen in this figure. First, all the three subsample have mild bluing trend in $M_{2000} - M_{K'}$ with increasing redshift as expected from our results on rest-LFs. For example, $M_{K'} \leq -23.5$ sample has median color $M_{2000} - M_{K'} = 7.46$ around $z = 0.3$, while at $z = 2.7$ there are no such red galaxies and median color becomes as blue as 4.73. The bluing trend we found has already been indicated by several studies (e.g., Cowie et al. 1996; Papovich, Dickinson, & Ferguson 2002) and is as qualitatively expected

from passive evolution model. Papovich, Dickinson, & Ferguson (2002) suggests that the UV-optical rest-frame SEDs of the Lyman break galaxies at $2.0 \lesssim z \lesssim 3.5$ are much bluer than those of present-day spiral and elliptical galaxies. Other two $-23.5 < M_{K'} \leq -21.0$ and $-21.0 < M_{K'} < -20.0$ subsamples also show this bluing trend at least at $z < 1.5$ and almost no color changes have been found beyond $z = 1.5$. Our sample is so small that we cannot discriminate the difference of rapidity of this bluing trend among subsamples.

It should be noted that an observational limit might affect this diagram. It is difficult to show explicitly the observational limit of $K' \leq 24.0$ in this rest-frame plane. For simplicity, we show in Figure 8 a fiducial line (thick solid line) denoting the bluer color limit of a galaxy having constant luminosity of $M_{2000} = -20$ which can be observed in the K' -band image ($K' \leq 24.0$), ignoring the small k -correction (e.g., Mannucci et al. 2001) at the K' -band. Galaxies brighter than $M_{2000} = -20$ would be detectable above this line. For a galaxy with $M_{2000} = -19$, you may shift the lower limit upward by 1mag. In higher redshift, it is found that galaxies which are bluer and fainter in 2000Å are hard to stay in this K' -limited sample. Our subsample of $-23.5 < M_K \leq -21.0$ and $-21.0 < M_K < -20.0$ would have been affected by this observational bias which may cause a lack of blue galaxies at high redshift if such blue population really exists. The bluing trend of these subsample seems to stop at $z = 1.5$ in Figure 8, though it may be possibly attributed to this bias.

On the other hand, for $M_K \leq -23.5$ subsample which seems to be less affected by this bias, all the galaxies become redder with time in $z < 1$, while there are galaxies around $z \simeq 1$ as blue as those at $z \simeq 3$. It seems that the scatter of the color becomes larger in nearby universe. The same trend can be seen in the rest-frame ($U - B$) color of brightest ($M_B < -20.3$) galaxy sample in HDF by Dickinson (2000). These galaxies with similar stellar masses keep their blue color against the passive evolution during longer timescale than typical timescale of an intense starburst event. This infers that a merging process (e.g., Lacey & Cole 1993) and subsequent star formation have been taken continuously during $1 \lesssim z \lesssim 3$ epoch. These blue galaxies of $M_K \leq -23.5$ at $z = 1$ seems to be assembled from lower mass galaxies via. merging and are on-going star formation.

Second, it is found that more massive galaxies tend to be redder in rest $M_{2000} - M_{K'}$ color at every epoch. The median color of massive galaxies is always redder than that of less massive galaxies. The trend that red galaxies are more luminous than blue ones has already been established in the local universe for example by Blanton et al. (2001), who found that high surface brightness, red, and highly concentrated galaxies are found to be on average more luminous than low surface brightness, blue, less concentrated galaxies. If rest $M_{2000} - M_{K'}$ color indicates the age of a galaxy, the massive galaxies tend to have older age, which can be easily inferred in the context of downsizing hypothesis, in which

massive (spheroidal) galaxies formed at high- z , followed at later epochs by the formation of less massive galaxies.

6. Contribution to the Global Star Formation Rate Density

In the last few years, there has been great advance in understanding the evolution of the global star formation rate density (SFRD). At low redshift between $z = 0$ and $z = 1.5$ the SFRD is found to be steadily increasing with redshift. At high redshift, some results (e.g., Madau, Pozzetti, & Dickinson 1998) meets the SFRD peak around $z \sim 1.5$, while others (e.g., Steidel et al. 1999) maintain it keeping relatively constant. The estimate of SFRD based on the ultraviolet luminosity of galaxies is strongly affected not only by dust obscuration which many investigators took into account but also by the faint end of the LF. At last in this study, we derive the SFRD based on our evaluated rest-UV LF.

The SFRD can be estimated by integrating over the best-fit Schechter function to infinity for rest-UV LF in each redshift bin. The following equation was used to convert luminosity at 2000Å, L_{2000} to SFR based on the calibration given by Madau, Pozzetti, & Dickinson (1998) for the case of a Salpeter IMF,

$$SFR(M_{\odot}\text{yr}^{-1}) = 1.26 \times 10^{-28} L_{2000}(\text{ergs s}^{-1}\text{Hz}^{-1}). \quad (4)$$

The result is represented in Figure 9, in which several previous estimates are also plotted. All the previous results except Steidel et al. (1999) were derived by integrating the Schechter function to infinity. For consistency, we increased the Steidel et al. (1999) points by an additional factor 1.7 as they have noted in the case of integration to infinity. We have checked our data point by recalculating the SFRD from other rest-UV wavelength such as 1500Å and 2800Å as was adopted in previous studies and found that our SFRD estimate is stable within a fluctuation of 0.2. The dust extinction is uncorrected in all the estimates.

Our results are denoted as solid circles and is broadly consistent with others at $z < 1.5$, though it show slight deficiencies at $z > 1.5$ where there are yet no established observations. This has probably arisen from the fact that our estimated rest-UV LF of K' -selected sample has shallower faint end slope than that of Steidel et al. (1999). For an attempt, if we change the LF slope at $2.5 < z \leq 3.5$ from $\alpha = -0.83$ to $\alpha = -1.6$ as Steidel et al. (1999) have adopted at $z = 3$, our estimate at $z = 3$ in Figure 9 shifts up to the open circle which is almost consistent with Steidel et al. (1999). Otherwise, if the slope of the rest-UV LF at $z = 3$ is really as steep as $\alpha = -1.6$, our $K' < 24.0$ limited sample contribute only 42% of the total UV luminosity density, namely, of the total star formation rate density at $z = 3$. The

remaining 58% should be charged to faint galaxies with $M_{2000} > -19$ in which our sample seems to have a deficiency of galaxies compared with the LF derived by Steidel et al. (1999). These missed faint galaxies correspond to very blue galaxies which are probably affected by observational limit in K' band as has been shown in §5. However, we should note here that the α derived by Steidel et al. (1999) has a large uncertainty as they have mentioned because it is determined only at the bright end ($M_{1700} < -20$) of the LF. Poli et al. (2001) have estimated the photometric redshifts for I -selected galaxies and obtained a shallower faint end slope $\alpha = -1.37 \pm 0.20$ for the rest-1700Å LF of $2.5 < z \leq 3.5$ galaxies down to $M_{1700} = -19$. The existence of a substantial population of such faint ($M_{1700} > -20$) and blue Lyman break galaxies at $z > 3$ is still questionable.

7. Summary

We have constructed the deepest K' -selected multi-color $BVRIz'JK'$ sample of field galaxies on Subaru Deep Field. Based on this multi-color data, a photometric redshift for each sample galaxy was estimated. Our principal conclusions are the following.

1. The overall $N(z)$ distribution for $K' \leq 21$ sample is consistent with previous observations, and we for the first time derived the $N(z)$ down to $K' = 24$. Taking account of dust extinction and selection effects of the sample, the observed $N(z)$ distribution at the most secure magnitude bin $22 < K' \leq 23$ is well described with PLE model, while a recent version of hierarchical galaxy formation model shows an apparent deficiency of galaxies, especially at $z > 2$. The PLE model with realitic dust evaluation can account for the abundance of the high- z ($z > 2$) galaxies. In the faintest $23 < K' \leq 24$ bin of $N(z)$, both of the model predictions are found to be inconsistent with the observation. The discrepancy in the faintest bin is presumably caused by the photometric errors that give an incorrect solution of photometric redshifts.
2. The rest K' , B , and UV(2000Å) band luminosity functions and their evolution have been investigated. The rest K' -band luminosity function shows almost no evolution up to $z = 3$. The rest- B luminosity function shows mild brightning with epoch up to $z = 2.5$, though its brightening degree is within the M^* error caused by photometric and redshift errors. The rest-2000Å LFs also show a luminosity evolution which is more significant than in the rest- B LF and continues up to $z = 3.5$. The M_{2000}^* value is getting luminous from $z = 0.6$ to $z = 3.5$ over 1 mag, which is more significant than M_{2000}^* errors.
3. The evolutionary trend of rest luminosity functions appears to correspond to the bluing

trend of the rest ($UV - K'$) color with increasing redshift. We also found that more massive galaxies are redder at every epoch.

4. The findings on the evolution of rest luminosity functions are qualitatively in favor of the PLE model. The star formation activity in a galaxy changes the rest blue luminosity while the amount of old stellar population does not change. The resulting rest K' -band luminosity function showing almost no evolution up to $z = 2.5$ can also be consistent with the hierarchical galaxy formation model if M/L_K decreases with redshift, that is, the number density of K' -band luminosity selected galaxies does not significantly change with redshift while the number density of stellar-mass selected galaxies decreases with look-back time.
5. We have evaluated the contribution to the cosmic star formation rate density of our K' -selected galaxies. The star formation rate density derived from integration of our rest-UV luminosity function is about 42% of that derived from Lyman break galaxies at $z = 3$. The result suggests a possibility that large fraction of global star formation rate density at $z > 2$ could come from the contribution of faint blue galaxy population at high- z universe which have not yet explicitly been identified.

Though the present results rely heavily on an availability of photometric redshifts, we are confident that we have successfully derived a coherent picture of evolution of K' , B , and UV rest-frame luminosity functions over $0.6 < z \leq 3.5$ to the faint end below the limit of the today's spectroscopic studies. Our result raises a question of how such massive galaxies have formed at high redshift with efficient star formation, which is apparently consistent with the PLE picture in the K -band, within the framework of the structure formation in the CDM universe. Of course, deeper NIR imaging surveys in future allows us to derive more secure results on $N(z)$ at the faintest magnitude and on faint end of the rest-LFs in which we have obtained robust results in this study. Deep observation at longer wavelength with *SIRTF* and *ASTRO-F* will be also required to constraint the SEDs of galaxies at $z > 3$. The technique that we have adopted in this study will be applied to future wide-field K -band survey to determine the rest luminosity at any wavelength at any redshift down to the faintest magnitude. On the other hand, on-going large multi-object spectroscopic surveys are of course extremely important to reveal the galaxy evolution more reliably.

We deeply appreciate the devoted support of the Subaru Telescope staff for this project. The research is supported the Ministry of Education, Science and Culture through Grant-in-Aid 11691140.

REFERENCES

Arimoto,N., & Yoshii,Y. 1987, A&A, 173, 23

Arimoto,N., Yoshii,Y., & Takahara,F. 1992, A&A, 253, 21

Barger,A.J., Cowie,L.L., Trentham,N., Fulton,E., Hu,E.M., Songaila, A., & Hall,D. 1999, AJ, 117, 102

Bertin,E., & Arnouts,S. 1996, A&AS, 117, 393

Bolzonella,M.J., Miralles,M., & Pello,R. 2000, A&A, 363, 47

Blanton,M.R., et al. 2001, AJ, 121, 2358

Bruzal,G., & Charlot,S. 1993, ApJ, 405, 538

Calzetti, D., Armus, L., Bohlin, R.C., Kinney, A.L., Koornneef, J., & Storchi-Bergmann, T., 2000, ApJ, 533, 682

Cole,S., et al. 2001, MNRAS, 326, 255

Connolly,A.J., Szalay,A.S., Dickinson,M.E., SubbaRao,M.U., & Brunner, R.J. 1997, ApJ, 486, L11

Cowie,L.L., Songaila,A, & Barger,A.J. 1999, AJ, 118, 603

Cowie,L.L., Songaila,A, Hu,E.M., & Cohen,J.G. 1996, AJ, 112, 839

Dickinson,M. 2000 in *Building Galaxies: From the Primordial Universe to the Present*, Proceedings of the XIXth Moriond Astrophysics Meeting, eds. F. Hammer, T.X. Thuan, V. Cayatte, B. Guiderdoni, & J. Tranh Than Van, (Paris: Ed. Frontieres), p. 257

Drory,N., et al., 2001, ApJ, 562, L111

Ellis,R.S., Colless,M., Broadhurst,T., Heyl,J., & Glazebrook,K. 1996, MNRAS, 280, 235

Felten,J.E. 1977, AJ, 82,861

Folkes,S., et al. 1999, MNRAS, 308, 459

Fontana,A., D'Odorico,S., Poli,F., Giallongo,E., Arnouts,S., Cristiani,S., Moorwood,A., & Saracco,P. 2000, AJ, 120, 220

Fontana,A., Menci,N., D'Odorico,S., Giallongo,E., Poli,F., Cristiani,S., Moorwood,A., & Saracco,P. 1999, MNRAS, 310, L27

Furusawa,H., et al. 2002 (Paper IV) in preparation.

Kashikawa,N., et al. 2000, SPIE, 4008, 104

Kauffmann,G., & Charlot, S. 1998, MNRAS, 297, L23 (KC98)

Lacey,C., & Cole,S. 1993, MNRAS, 1993, 262, 627

Lowenthal,J.D., et al. 1997, ApJ, 481, 673

Lilly,S.J., Le Févre,O., Hammer,F., & Crampton,D. 1996, ApJ, 460, L1

Lilly,S.J., Tresse,L., Hammer,F., Crampton,D., & Le Févre,O. 1995, ApJ, 455, 108

Loveday,J. 2000, MNRAS, 312, 517

Maihara,T., et al. 2001, PASJ, 53, 25 (Paper I)

Madau,P., Pozzetti,L., & Dickinson,M. 1998, ApJ, 498, 106

Madau,P., 1995, ApJ, 441, 18

Mannucci,F., Basile,F., Poggianti,B.M., Cimatti,A., Daddi,E., Pozzetti,L., & Vanzi,L. 2001, MNRAS, 326, 745

Miyazaki,S., Sekiguchi,M., Imi,K., Okada,N., Nakata,F., & Komiyama,Y. 1998, SPIE, 3355, 363

Nagashima,M., Yoshii,Y., Totani,T., & Gouda,N. 2002, ApJ, in press.

Nagashima,M., Totani,T., Gouda,N., & Yoshii,Y. 2001, ApJ, 557, 505

Ouchi, M. et al. 2002, ApJ, submitted (Paper II)

Papovich,C., Dickinson,M., & Ferguson,H.C. 2002, astro-ph/0201221

Poli,F., Menci,N., Giallongo,E., Fontana,A., Cristiani,S., & D'Odorico,S. 2001, ApJ, 551, L45

Rudnick et al. 2001, AJ, 122, 2205

Saracco,P., et al. 2001, A&A, 375, 1

Sawicki,M.J., Lin,H., & Yee,K.C. 1997, AJ, 113, 1

Schlegel,D.J., Finkbeiner,D.P., & Davis,M. 1998, ApJ, 500, 525

Shapley,A.E., Steidel,C.C., Adelberger,K.L., Dickinson,M., Giavalisco,M., & Pettini,M. 2001, ApJ, 562, 95

Shimasaku,K. et al. in preparation.

Steidel,C.C., Adelberger,K.L., Giavalisco,M., Dickinson,M., & Pettini,M. 1999, ApJ, 519, 1

Steidel,C.C., Giavalisco,M., Dickinson,M., & Adelberger,K.L. 1996, AJ, 112, 352

Sullivan,M., Treyer,M.A., Ellis,R.S., Bridges,T.J., Milliard,B., & Donas,J. 2000, MNRAS, 312, 442

Totani,T., Yoshii,Y., Iwamuro,F., Maihara,T., & Motohara,K. 2001a, ApJ, 550, L137

Totani,T., Yoshii,Y., Iwamuro,F., Maihara,T., & Motohara,K. 2001b, ApJ, 559, 592

Totani, T. & Yoshii, Y. 2000, ApJ, 540, 81

Yoshii, Y. 1993, ApJ, 403, 552

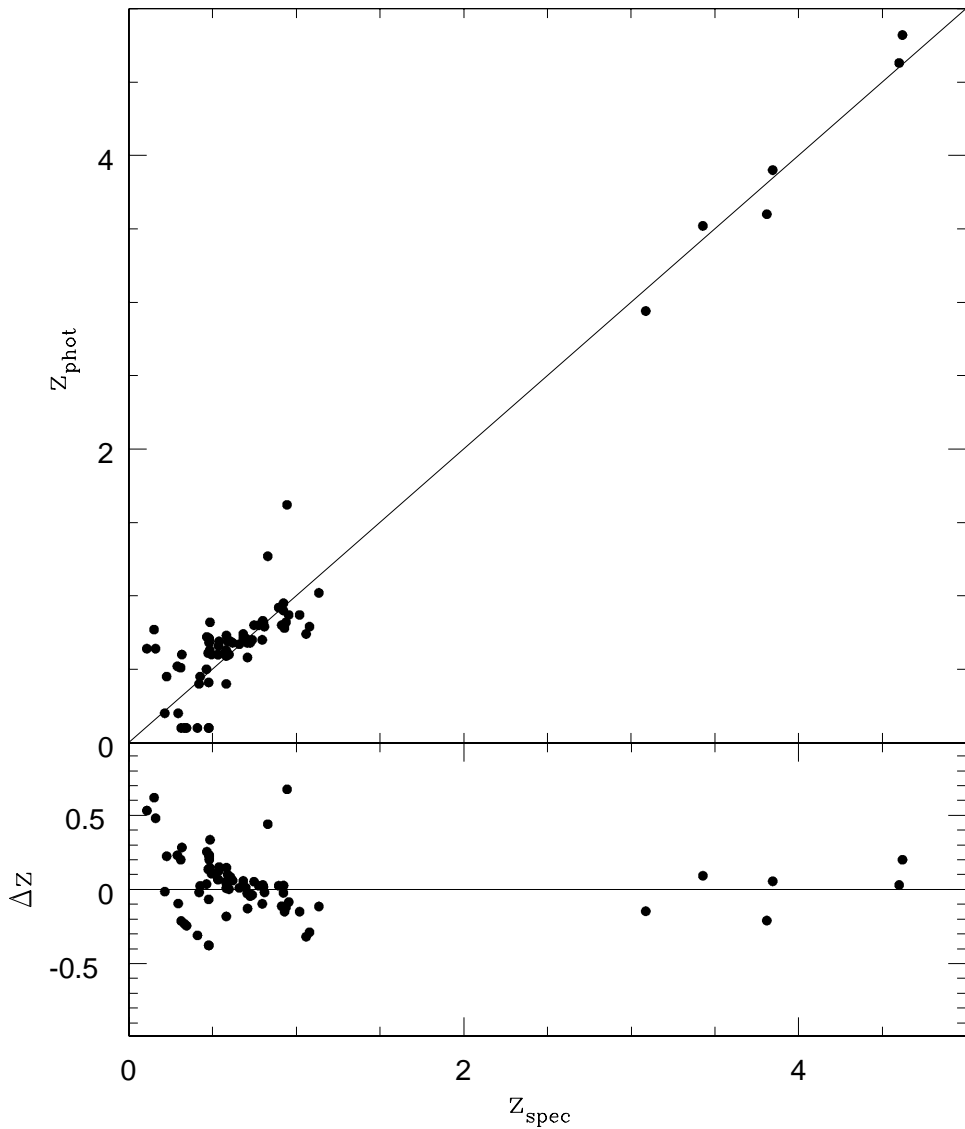


Fig. 1.— Comparison between z_{spec} and z_{phot} for our spectroscopic sample of SDF.

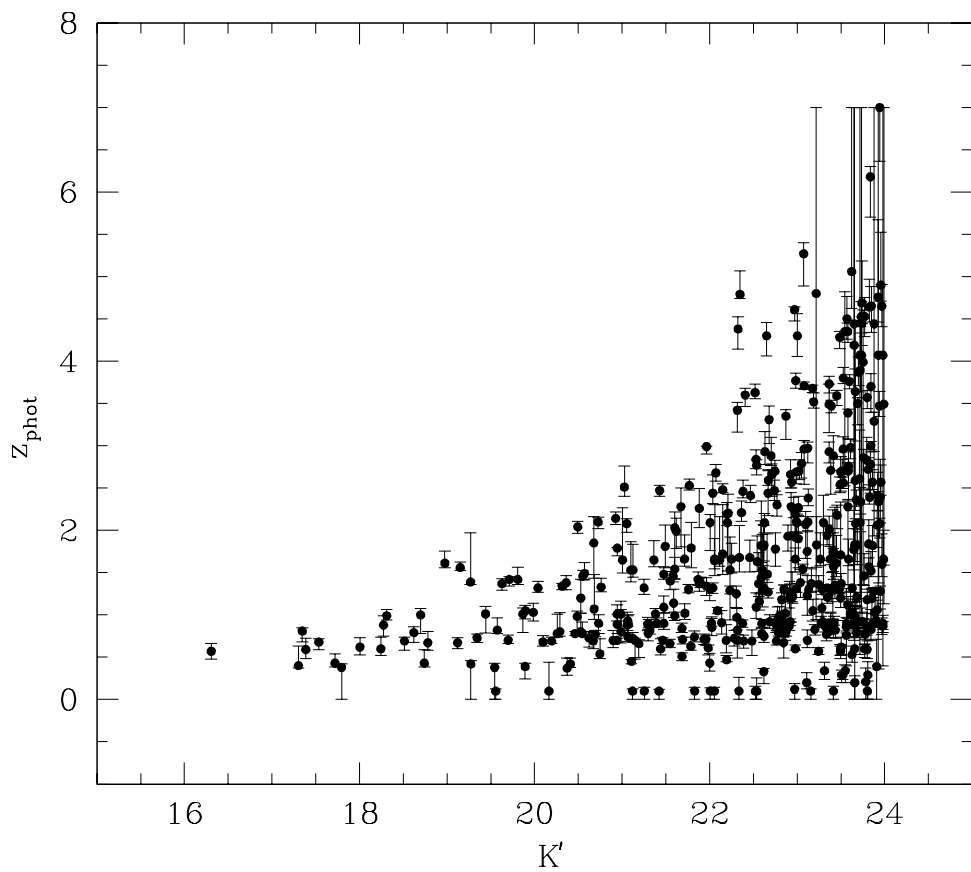


Fig. 2.— K' magnitude vs. z_{phot} diagram. The error bars of photometric redshifts are evaluated from χ^2 probability distribution with the confidence level at 90%.

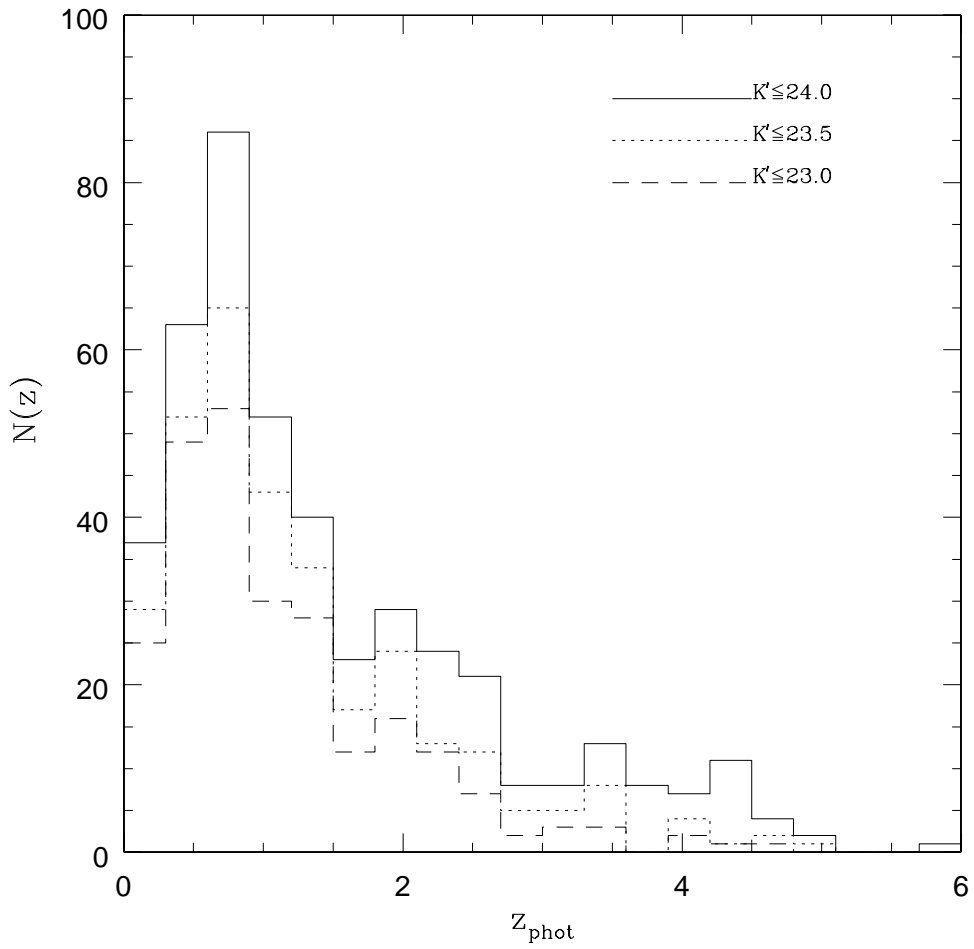


Fig. 3.— The redshift distribution of our SDF sample with different limiting magnitudes of $K' \leq 23.0$, $K' \leq 23.5$, and $K' \leq 24.0$.

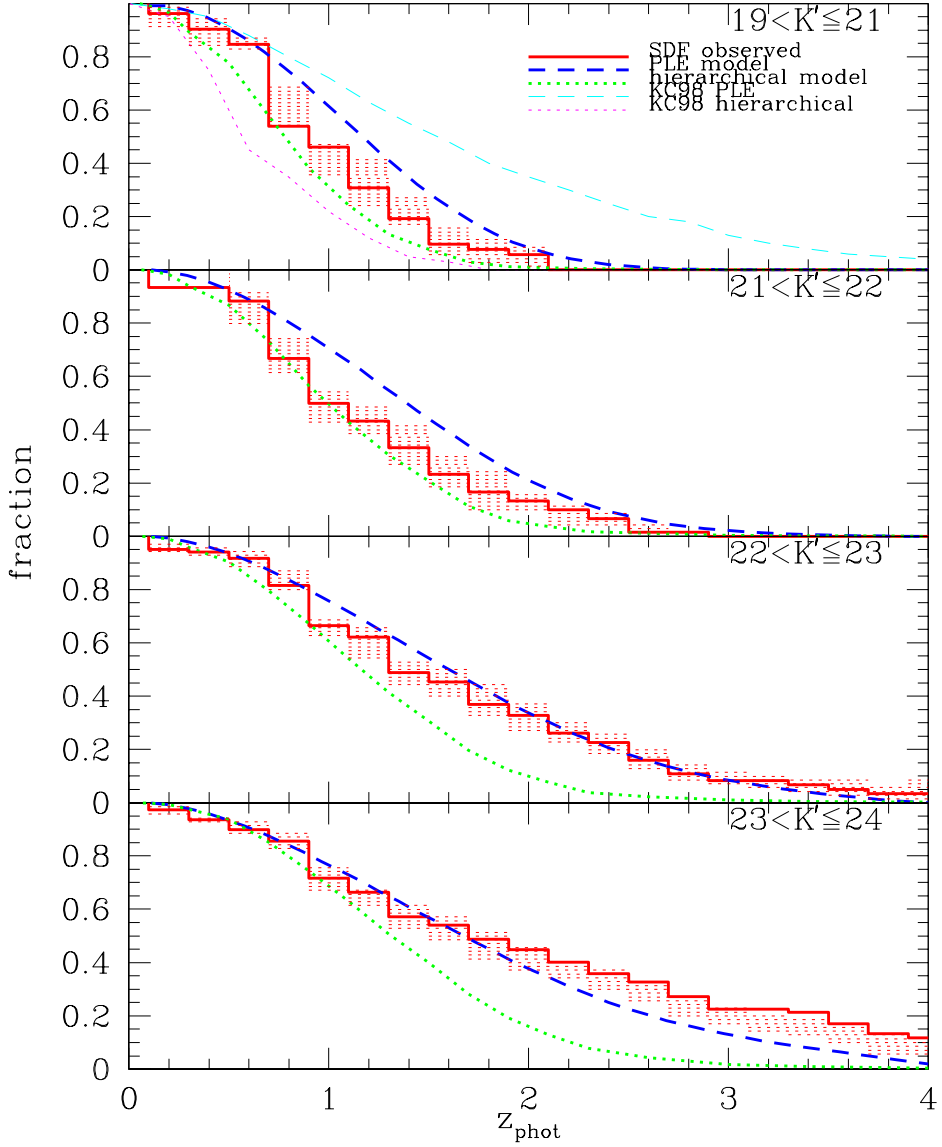


Fig. 4.— The normalized cumulative redshift distribution for our SDF sample for the bright magnitude bin to the faint from top to bottom panel. The thick solid histograms show the results of observation. The shaded regions show the $\pm 3\sigma$ deviated counts estimated by Monte Carlo realizations when photometric redshift errors are taken into account. The thick dashed lines denote the prediction of the PLE model by Totani et al.(2001b), while the thick dotted lines denote the the hierarchical galaxy formation model by Nagashima et al.(2002). The prediction of PLE and hierarchical clustering models in KC98 are also shown in the top panel.

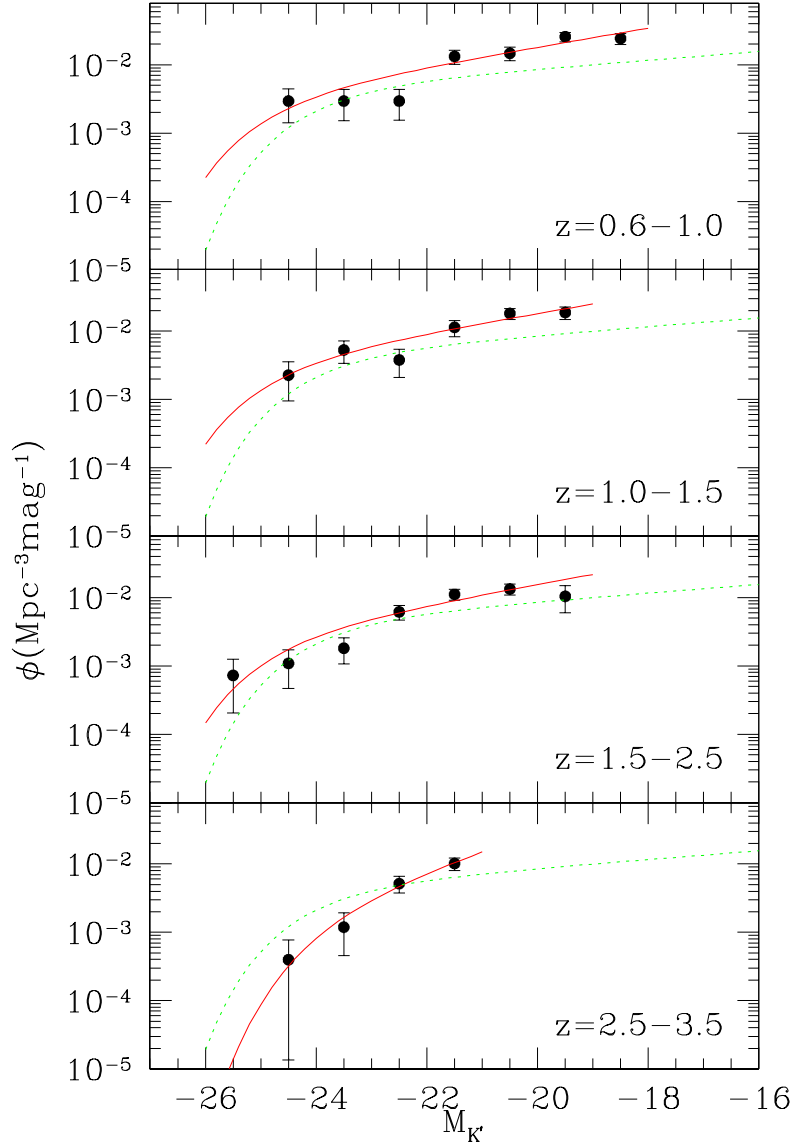


Fig. 5.— The rest K' -band luminosity functions at $z = 0.6 - 1.0$, $z = 1.0 - 1.5$, $z = 1.5 - 2.5$, and $z = 2.5 - 3.5$ from top to bottom. The solid circles show determined luminosity function in the present study, and solid lines are the best fit Schechter functions. The dotted line shows the local K' luminosity function by Loveday (2000)

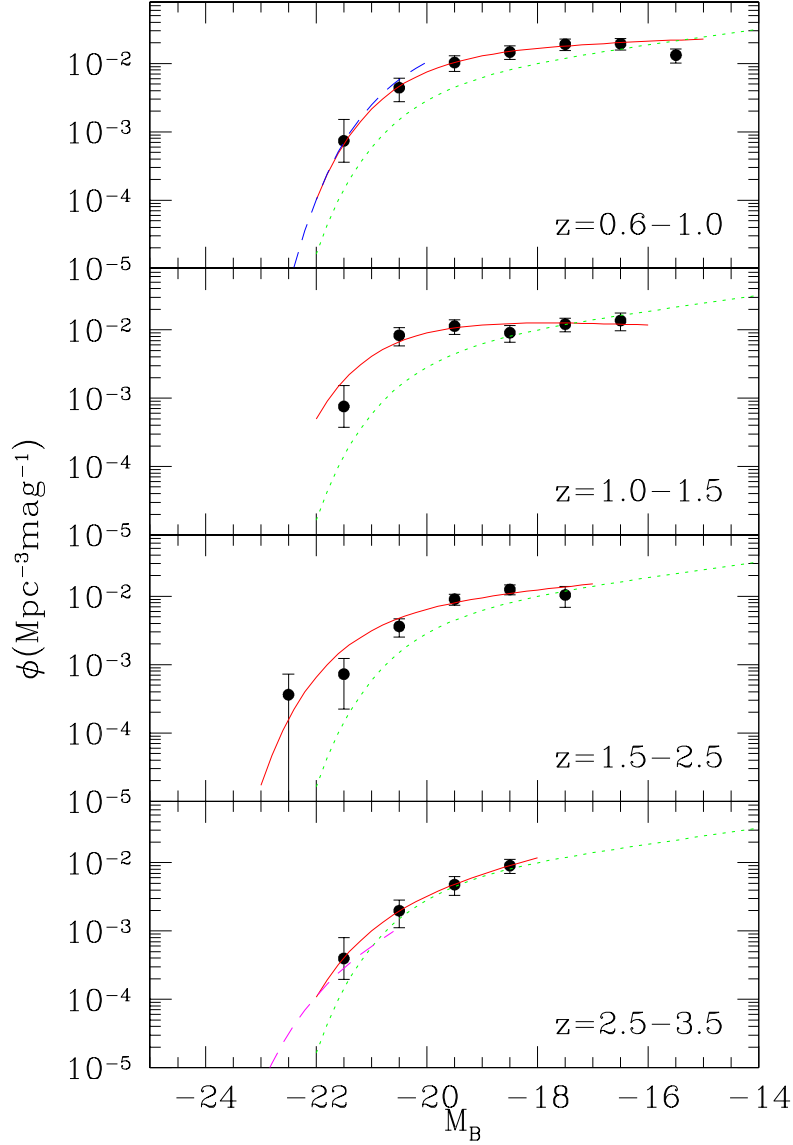


Fig. 6.— Same as Figure 5 for rest B -band LFs. The local B -band luminosity function denoted as dotted line is from Blanton et al. (2001) converted from their g^* band to B band. In the top panel, $0.75 < z < 1.0$ rest B -band LF derived on CFRS (Lilly et al. 1995) is also superimposed as a dashed line. In the $2.5 < z < 3.5$ panel, a dashed line shows the rest V -band LF for Lyman-break galaxies at $\langle z \rangle = 3.04$ by Shapley et al. (2001) converted to rest- B band and $\Omega_m = 1.0$, $h = 0.75$ cosmology.

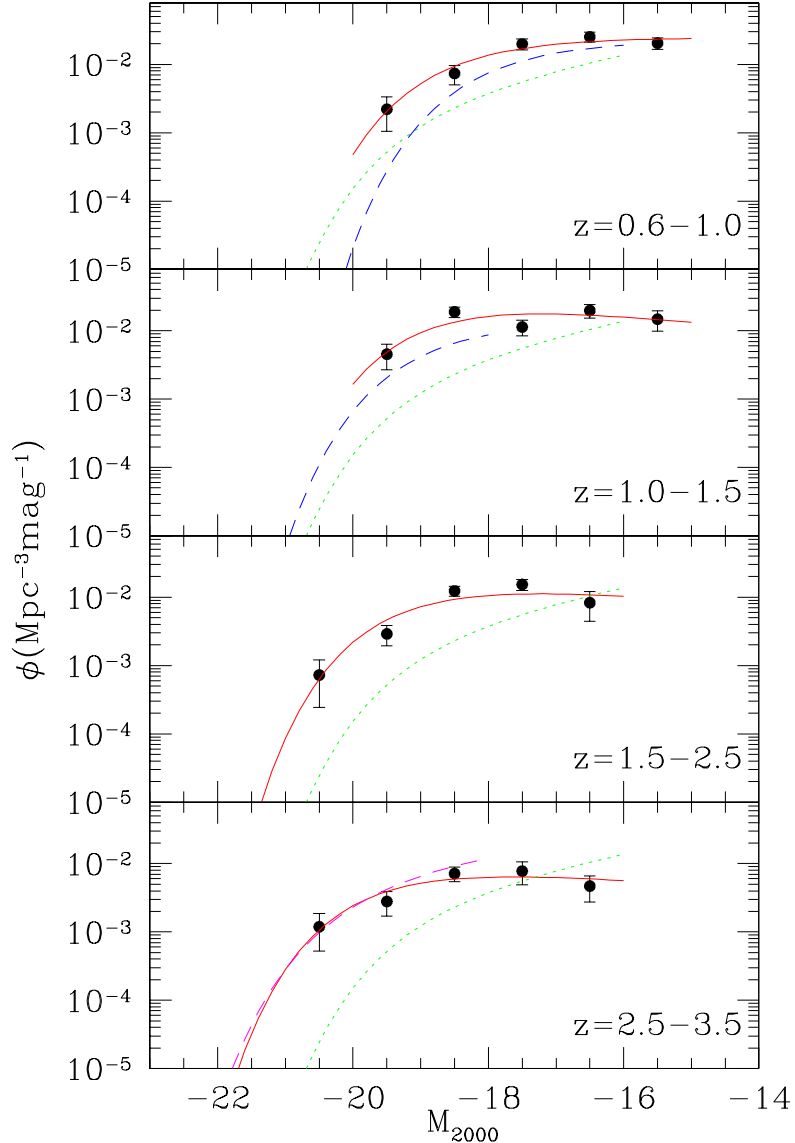


Fig. 7.— Same as Figure 5 for rest UV(2000Å *AB*)-band LFs. The local 2000Å luminosity function by Sullivan et al. (2000) in the case of $h = 0.75$ is denoted as dotted line converted their magnitude system to *AB* system with a 2.29 mag offset. In the $0.6 < z < 1.0$ and $1.0 < z < 1.5$ panels, dashed line shows the rest 2000Å LF for $0.5 < z < 0.9$ and $1.0 < z < 1.5$ derived by Cowie, Songaila, & Barger (1999) in the case of $\alpha = -1.0$ and $h = 0.75$. In the $2.5 < z < 3.5$ panel, a dashed line shows the rest 1700Å LF for Lyman-break galaxies at $\langle z \rangle = 3.04$ by Steidel et al. (1999).

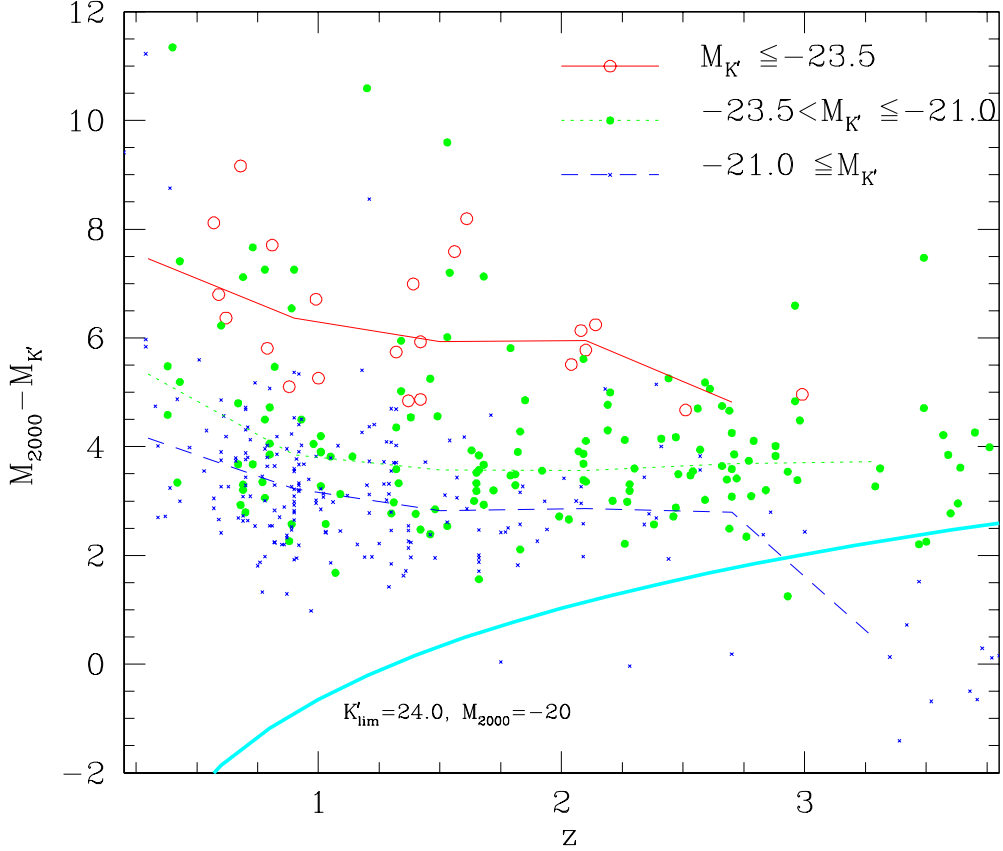


Fig. 8.— The rest $M_{2000} - M_{K'}$ color evolution with redshift. Open circles, small filled circles and cross dots denote the subsamples with respect to the absolute K' magnitudes, $M_{K'} \leq -23.5$, $-23.5 < M_{K'} \leq -21.0$ and $-21.0 < M_{K'}$ sample respectively. The median $M_{2000} - M_{K'}$ color for each redshift is traced by solid, dotted and dashed lines from bright subsample to faint subsample. We show a thick solid line as a fiducial line denoting the lower color limit corresponding to our sample's magnitude limit of $K'_{lim} = 24.0$ galaxy in the case of having constant $M_{2000} = -20$ ignoring the small k -correction at K' -band. Galaxies brighter than $M_{2000} = -20$ would be detectable above this line. If $M_{2000} = -19$ galaxy, you may shift the lower limit upper by 1mag.

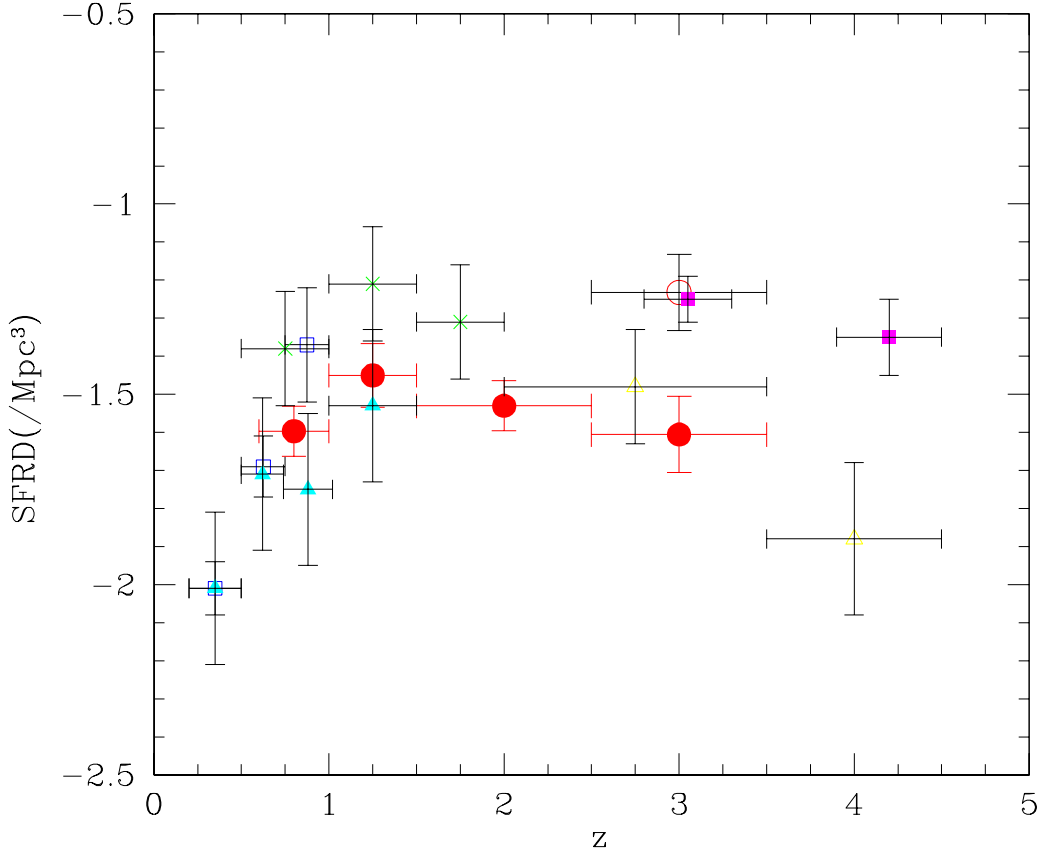


Fig. 9.— The star formation rate density as a function of redshift (Madau plot) derived from the integration of UV-LF. The estimates of this work are shown in filled circles. The different data are taken from previous estimates of Lilly et al. (1996) (open squares), Connolly et al. (1997) (crosses), Cowie et al. (1999) (filled triangles), Madau et al. (1998) (open triangles), and Steidel et al. (1999) (filled squares). The dust extinction is uncorrected in all the estimates. If we change our rest-UV LF slope from $\alpha = -0.83$ to $\alpha = -1.6$ as Steidel et al. (1999) have adopted at $z = 3$, the estimate at $z = 3$ shifts up to the open circle from the filled circle.

Table 1. Summary of Optical Imaging Data for SDF.

band	exp.time (sec)	seeing size (arcsec)	m_{lim}^a (mag)
<i>B</i>	9000	0.6	28.08
<i>V</i>	3600	0.8	26.28
<i>R</i>	14400	0.7	27.88
<i>I</i>	3600	0.7	25.93
<i>z'</i>	3600	0.8	24.27

^aThe 5σ limiting magnitudes in Vega system within $2''$ aperture

Table 2. Chance probability and χ^2 (in parentheses) values obtained from Kolmogorov-Smirnov Test for $N(z)$ Distribution.

models	$19 < K' \leq 21$	$21 < K' \leq 22$	$22 < K' \leq 23$	$23 < K' \leq 24$
PLE	1.97%(8.90)	1.03%(10.2)	18.2%(4.67)	0.232%(13.3)
hierarchical	9.32%(5.91)	76.4%(1.72)	6.46e-4%(24.7)	4.49e-13%(66.2)

Table 3. The Best Fit Schechter Parameters of Rest-Frame Luminosity Functions in Each Redshift Bin Derived on SDF

rest-frame	z range	α	M^*	ϕ^*
K'	0.6 – 1.0	$-1.35^{+0.05}_{+0.02}$	$-25.03^{+0.12}_{-0.27}$	$3.87^{+2.12}_{-0.41} \times 10^{-3}$
	1.0 – 1.5	$-1.35^{+0.01}_{-0.10}$	$-25.02^{+0.49}_{-0.05}$	$3.87^{+0.94}_{-2.18} \times 10^{-3}$
	1.5 – 2.5	$-1.37^{+0.09}_{+0.00}$	$-24.95^{+0.22}_{+0.01}$	$3.13^{+2.09}_{+0.09} \times 10^{-3}$
	2.5 – 3.5	$-1.70^{+0.17}_{-0.06}$	$-23.95^{+0.11}_{-0.35}$	$2.57^{+1.88}_{-1.75} \times 10^{-3}$
B	0.6 – 1.0	$-1.07^{+0.01}_{-0.07}$	$-20.26^{+0.26}_{-0.63}$	$1.76^{+0.14}_{-0.67} \times 10^{-2}$
	1.0 – 1.5	$-0.92^{+0.13}_{-0.10}$	$-20.61^{+0.19}_{+0.31}$	$1.80^{+0.30}_{-0.70} \times 10^{-2}$
	1.5 – 2.5	$-1.19^{+0.25}_{+0.01}$	$-21.10^{+0.37}_{+0.01}$	$8.31^{+7.82}_{+1.76} \times 10^{-3}$
	2.5 – 3.5	$-1.49^{+0.45}_{-0.01}$	$-20.82^{+0.44}_{-0.30}$	$3.86^{+6.84}_{-3.49} \times 10^{-3}$
$U(2000\text{\AA})$	0.6 – 1.0	$-0.99^{+0.34}_{-0.11}$	$-18.49^{+0.31}_{-0.11}$	$2.79^{+0.80}_{-0.08} \times 10^{-2}$
	1.0 – 1.5	$-0.75^{+0.10}_{-0.04}$	$-18.71^{+0.07}_{-0.06}$	$3.49^{+0.08}_{-0.76} \times 10^{-2}$
	1.5 – 2.5	$-0.83^{+0.21}_{-0.04}$	$-19.12^{+0.18}_{-0.05}$	$1.95^{+0.88}_{+0.36} \times 10^{-2}$
	2.5 – 3.5	$-0.83^{+0.26}_{-0.13}$	$-19.54^{+0.23}_{-0.12}$	$1.11^{+0.67}_{-0.04} \times 10^{-2}$